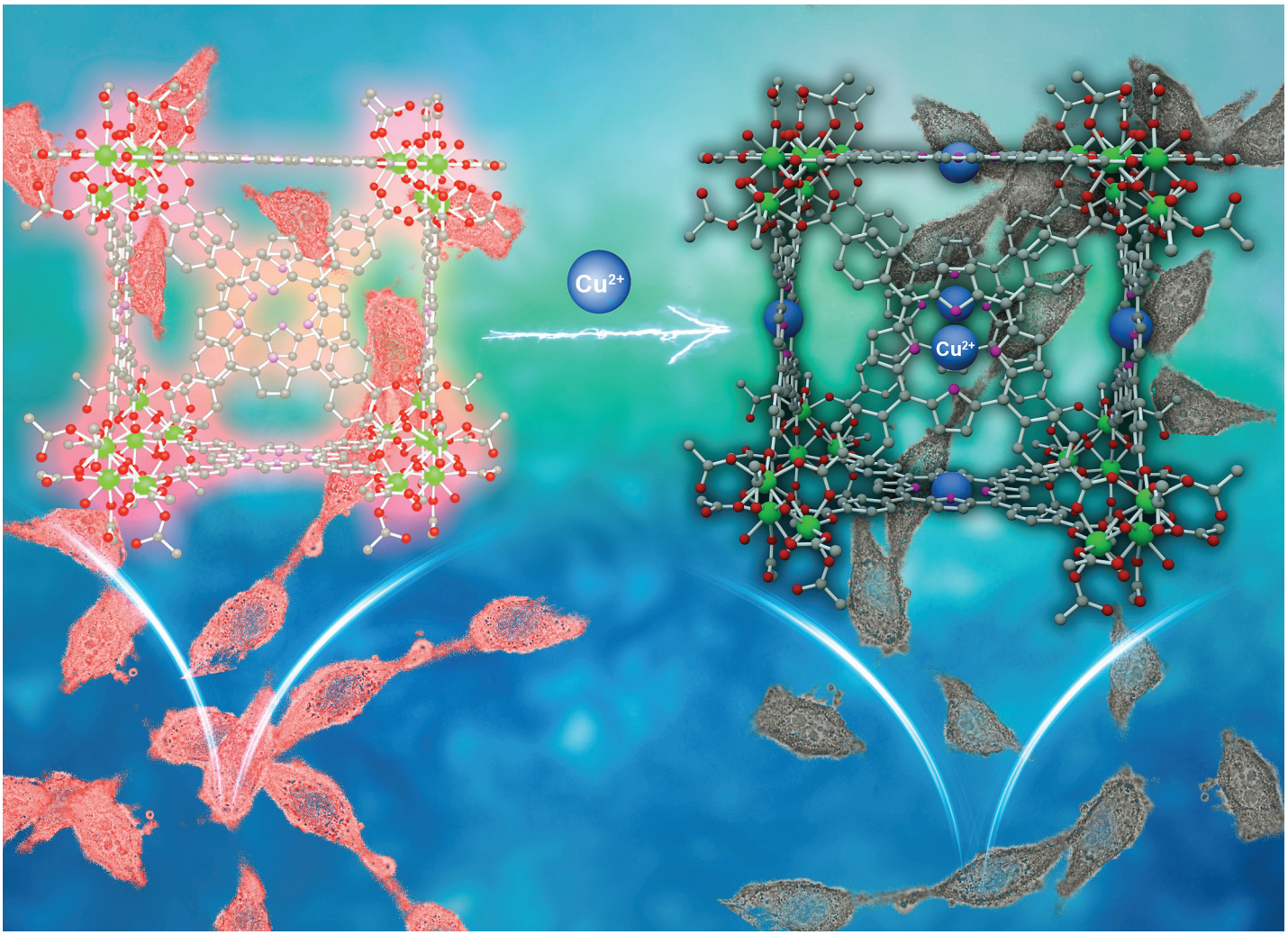


**Showcasing research on metal–organic framework nanoparticle-based fluorescent nanosensor for $Cu^{2+}$ detection from Professor Mo Yang's laboratory, Department of Biomedical Engineering, the Hong Kong Polytechnic University, Hong Kong SAR, PR China.**

An ultrasensitive and selective fluorescent nanosensor based on porphyrinic metal–organic framework nanoparticles for $Cu^{2+}$ detection

Porphyrinic metal–organic framework nanoparticles (*i.e.* MOF-525 NPs) with attractive properties including ultrasmall size, good water dispersity and intense fluorescence were prepared *via* a facile and environment-friendly hydrothermal route, and a sensitive and selective fluorescent nanosensor based on MOF-525 NPs was proposed for $Cu^{2+}$ monitoring in water and living cells.

## As featured in:

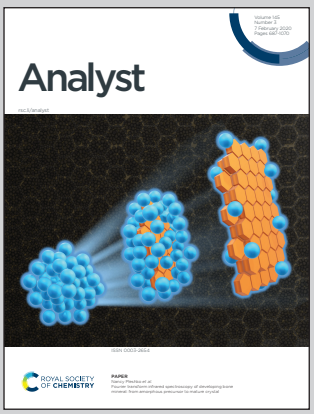


See Changming Cheng, Mo Yang *et al.*, *Analyst*, 2020, **145**, 797.

ROYAL SOCIETY OF CHEMISTRY

rsc.li/analyst

Registered charity number: 207890

Analyst

ROYAL SOCIETY OF CHEMISTRY

PAPER

View Article Online
View Journal | View Issue





Cite this: *Analyst*, 2020, **145**, 797

# An ultrasensitive and selective fluorescent nanosensor based on porphyrinic metal–organic framework nanoparticles for $Cu^{2+}$ detection†

Changming Cheng, *[a,b] Ruolin Zhang,[a] Jiuhai Wang,[a] Yu Zhang,[c] Chunyi Wen,[a] Youhua Tan [a] and Mo Yang*[a]

Received 7th November 2019,
Accepted 17th December 2019

DOI: 10.1039/c9an02231g

rsc.li/analyst

Detecting trace amounts of copper ions ($Cu^{2+}$) is of high importance since copper is an essential element in the environment and the human body. Despite the recent advances in $Cu^{2+}$ detection, the current approaches still suffer from insensitivity and lack of *in situ* detection in living cells. In the present work, a fluorescent nanosensor based on porphyrinic metal–organic framework nanoparticles (MOF-525 NPs) is proposed for sensitive and selective monitoring of $Cu^{2+}$ in aqueous solution and living cells. The MOF-525 NPs with attractive properties, including ultrasmall size, good water dispersity and intense red fluorescence, are prepared *via* a facile and environment-friendly hydrothermal route. The fluorescence signal of MOF-525 NPs could be quenched statically by $Cu^{2+}$ with high selectivity due to the strong affinity of $Cu^{2+}$ to the porphyrin ligand in MOF-525. The proposed fluorescent nanosensor has a linear response in the range of 1.0–250 nM with a low detection limit of 220 pM. Furthermore, it is successfully employed for the detection of $Cu^{2+}$ in water samples and the intracellular imaging of $Cu^{2+}$ in living cells, demonstrating its great potential in the sensing and biological fields.

## Introduction

In the chemical sensing and biosensing fields, $Cu^{2+}$ is of great interest due to its important role in the environment and biology. It is one of the common pollutants in water and excessive concentration of $Cu^{2+}$ in the body might cause damage to the liver and kidney. $Cu^{2+}$ is one of the essential metal elements in the human body and intracellular $Cu^{2+}$ is important for some biological processes such as enzyme activities. Both deficiency and excess of $Cu^{2+}$ in the human body would result in some diseases (*e.g.* Wilson's disease, Alzheimer's disease, and Parkinson's disease).[1,2] As such, it is highly desired to develop sensitive and selective sensing strategies for $Cu^{2+}$ monitoring in water samples and living cells.

The typical instrumental detection techniques (*e.g.*, atomic absorption spectrometry,[3] inductively coupled plasma mass spectrometry,[4] and atomic emission spectrometry[5]) could be applied for $Cu^{2+}$ analysis. However, they may suffer from bulky instrumentation and complicated operation procedures. In the previous work, we have proposed a graphite-like carbon nitride-based electrochemiluminescent sensor and a carbon nanosphere-based electrochemical sensor for the rapid and sensitive detection of $Cu^{2+}$, respectively.[6,7] However, these approaches are not suitable for intracellular $Cu^{2+}$ monitoring in living cells. Fluorescent sensors have attracted a lot of attention for $Cu^{2+}$ monitoring in aqueous solution and in the living system[2,8–13] because they are relatively sensitive and have a simple setup. Fluorescent nanosensors based on diverse nanomaterials such as carbon dots and quantum dots have been developed for $Cu^{2+}$ monitoring in living cells.[14,15] New fluorescent sensors with high sensitivity, good photostability and selectivity are highly desirable for $Cu^{2+}$ monitoring in living cells.

In the past few years, widespread attention has been paid to a newly emerging family of porous materials with diverse structures and intriguing chemical and physical properties – metal–organic frameworks (MOFs). It is well known that MOFs are extended networks with interconnections of variable inorganic metal nodes and organic ligands, while they would inherit the properties of both inorganic and organic moieties and exhibit

[a]*Department of Biomedical Engineering, the Hong Kong Polytechnic University, Hung Hom, Kowloon, Hong Kong SAR, PR China.*
*E-mail: chengcm2019@outlook.com, Mo.Yang@polyu.edu.hk*
[b]*Institute of Nuclear Physics and Chemistry, China Academy of Engineering Physics (CAEP), Mianyang, PR China*
[c]*Mechanical & Automotive Engineering, School of Engineering, RMIT University, Melbourne, Victoria 3004, Australia*

†Electronic supplementary information (ESI) available: Zeta potential of MOF-525 NPs, time-dependent fluorescence response of MOF-525 NPs in the presence of $Cu^{2+}$, cell viability of MOF-525 NPs, comparison of different fluorescent sensors for $Cu^{2+}$ detection, and determination of $Cu^{2+}$ in drinking water. See DOI: 10.1039/c9an02231g

great potential applications in the biomedical fields such as drug delivery, bioimaging, and sensing.[16,17] Recently, micro-sized and sub-micro-sized MOFs (*e.g.*, CPP-16, PCN-525, and UiO-66(OH)$_2$@PCN-224) have been used for the selective detection of $Cu^{2+}$ due to the strong affinity of $Cu^{2+}$ to ligands.[18–20] However, these MOFs are not suitable for *in situ* intracellular $Cu^{2+}$ imaging, since it is difficult for MOFs with big particle size to enter living cells, and the detection processes are primarily performed in organic solution.[18–20] Furthermore, compared with bulky or microsized MOFs, nanoscale MOFs (NMOFs) may exhibit distinguishing properties such as high surface area and abundant active sites. Until now, there were few reports on nanoscale MOF-based sensors for the intracellular imaging of $Cu^{2+}$.

In this paper, we proposed a fluorescent nanosensor based on porphyrinic metal–organic framework nanoparticles (MOF-525 NPs) for sensitive and selective monitoring of $Cu^{2+}$ in aqueous solution and living cells (Fig. 1). MOF-525 NPs were synthesized *via* a hydrothermal route by using a zirconium(IV) cluster and tetrakis(4-carboxyphenyl)porphyrin (TCPP) as the metal node and organic ligand, respectively. Recently, low-cost and environment-friendly water has been used as the green solvent instead of classical organic solvents for the preparation of several MOFs including MFM-300($V^{III}$),[21] Al-TCPP,[22] UiO-66-$NH_2$,[23] and HKUST-1.[24] However, to the best of our knowledge, there are few reports on the water-based synthesis of MOF-525 NPs. The synthesized MOF-525 NPs exhibited small size, intense red fluorescence emission and good water dispersity. In the presence of $Cu^{2+}$, the fluorescence signal of MOF-525 NPs was selectively quenched by $Cu^{2+}$ due to the unique affinity of $Cu^{2+}$ to the TCPP ligand. This MOF-525 NP-based fluorescent sensor would exhibit a linear response to $Cu^{2+}$ in the range of 1.0–250 nM with a low detection limit of 220 pM. Furthermore, the proposed fluorescent sensor was successfully employed for $Cu^{2+}$ sensing in water samples and intracellular imaging of $Cu^{2+}$ in living HeLa cells. The promising potential of MOF-525 NPs in chemical sensors and biology was well demonstrated.

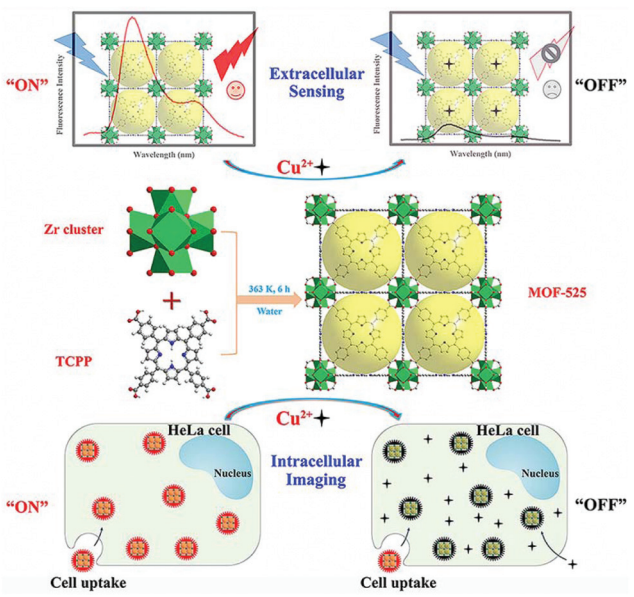


Fig. 1 Schematic illustration of the preparation of MOF-525 NPs and the "Signal-Off" fluorescence sensing for $Cu^{2+}$.

## Experimental

### Chemicals

Zirconium(IV) chloride ($ZrCl_4$, 98%), tetrakis(4-carboxyphenyl) porphyrin (TCPP, 97%), and copper(II) nitrate trihydrate (Cu$(NO_3)_2{\cdot}3H_2O$, 99.99%) were purchased from J&K Scientific Ltd (Beijing, China). Acetic acid (HAc, 99.99%), 3-(4,5-dimethylthiazol-2-yl)-2,5-diphenyltetrazolium bromide (MTT) and 4-(2-hydroxyethyl)-1-piperazineethanesulfonic acid (HEPES) buffer solution were purchased from Sigma (St Louis, MO, USA). Other chemicals were of analytical grade and used as received without further purification.

### Hydrothermal preparation of MOF-525 NPs

MOF-525 NPs were prepared according to the previous work with some modification.[25] Typically, $ZrCl_4$ (0.01 mmol) and HAc (0.175 mmol) were firstly dissolved in 14.4 mL of deionized water, followed by dropwise addition of TCPP (0.004 mmol) which was dissolved in 1.6 mL of NaOH solution (0.02 M). After stirring for 10 min, the resulting mixture solution was transferred into a 20 mL autoclave and heated in an oven at 363 K for 6 h. After cooling down to room temperature, the sample was collected by centrifugation, and washed with anhydrous ethanol and deionized water several times. Finally, the obtained product was re-dispersed in deionized water for further use.

### Characterization

The powder XRD pattern was recorded using a Rigaku SmartLab diffractometer (Tokyo, Japan) using Cu Kα source irradiation. The TEM image was obtained using a JEOL Model JEM-2100F field emission electron microscope (Tokyo, Japan). UV-vis absorption spectra were recorded on a Shimadzu UV-vis spectrophotometer (Kyoto, Japan). Fluorescence spectra and fluorescence decay curves were obtained using an Edinburgh FLS920 photoluminescence spectrometer (Edinburgh, UK). Confocal fluorescence images were obtained using an Olympus FV1000-IX81 confocal laser scanning biological microscope (Tokyo, Japan) and a Leica TCS-SP5 confocal system (Heidelberg, Germany). MTT assay was performed using a Tecan Infinite 200 microplate reader (Männedorf, Switzerland).

### Fluorescence sensing of $Cu^{2+}$ in aqueous solution

Fluorescence sensing of $Cu^{2+}$ was carried out in HEPES buffer solution (20 mM, pH 7.4) in the presence of MOF-525 NPs (5 mg $L^{-1}$). The MOF-525 NP dispersion was incubated with $Cu^{2+}$ solution at different concentrations for 180 min, and then the fluorescence spectra in the wavelength range of

600–750 nm under an excitation wavelength of 414 nm were recorded. In order to evaluate the selectivity of the MOF-525 NP-based fluorescent nanosensor, the possible interference of other common metal ions (*e.g.*, $Mg^{2+}$, $Zn^{2+}$, $Ca^{2+}$, $Cd^{2+}$, $Fe^{2+}$, $Fe^{3+}$, $Ni^{2+}$, $Ag^{+}$, $Al^{3+}$, $Hg^{2+}$, $Co^{2+}$, and $Pb^{2+}$) was investigated.

### Cell viability of MOF-525 NPs

MTT assay was conducted to evaluate the cytotoxicity of MOF-525 NPs to HeLa cells. Firstly, HeLa cells were seeded in a 96-well plate at a density of $1.0 \times 10^4$ cells per well and cultured in Dulbecco's modified Eagle's medium in the presence of 10% fetal bovine serum and 1% penicillin/streptomycin in an incubator (37 °C, 5% $CO_2$) for 24 h. Then, MOF-525 NPs with different concentrations (10–60 mg $L^{-1}$) were added into the wells (100 μL per well) and cultured for 24 h. After discarding the solution, 100 μL of cell medium containing MTT (10 μL, 5 g $L^{-1}$) was added into each well, and further incubated for 4 h. Then, 100 μL of dimethyl sulfoxide was added into each well to replace the cell medium, and another 10 min incubation was performed. The control group was subjected to the same procedure in the absence of MOF-525 NPs. Finally, the absorbance value at a wavelength of 490 nm in each well was recorded and the cell viability was calculated with the following formula (1):

$$\text{Cell viability } (\%) = (A_s - A_b)/(A_c - A_b) \times 100\% \quad (1)$$

where $A_s$, $A_b$, and $A_c$ are the absorbance values of the experimental group, the blank well and the control group, respectively.

### Intracellular imaging of $Cu^{2+}$

Prior to intracellular $Cu^{2+}$ imaging, HeLa cells were cultured in Petri dishes at a density of $1.0 \times 10^6$ cells per well and incubated with 30 mg $L^{-1}$ MOF-525 NPs for 1 h at 37 °C (5% $CO_2$). After incubation, the HeLa cells were washed with PBS three times. Then, exogenous $Cu^{2+}$ solution with a final concentration of 0–50 μM was added and incubated with the HeLa cells for another 1 h. The control cell group was subjected to the same procedure in the absence of MOF-525 NPs and $Cu^{2+}$. After washing with PBS three times, confocal fluorescence images of the HeLa cells were obtained in the wavelength range of 550–800 nm under an excitation wavelength of 405 nm. Similar protocols were widely employed in previous studies for intracellular imaging of $Cu^{2+}$.[14,26]

## Results and discussion

### Synthesis and characterization of MOF-525 NPs

In this work, for the first time, a facile and environment-friendly hydrothermal route was successfully employed for the preparation of ultrasmall fluorescent MOF-525 NPs. The morphology and size of the as-prepared sample were characterized by TEM (Fig. 2a). It could be observed clearly that the products were nearly spherical crystals with an average size of 5 nm, as revealed in the insets of Fig. 2a. The ultrasmall size of the as-prepared sample could be attributed to the low concentration of precursors and relatively mild reaction conditions, similar to our previous work.[27] It is worth pointing out that the cubic crystal with a regular shape and a sharp edge of typical MOF-525 was not observed in the present work probably due to the ultrasmall size. Similar phenomena have been reported in previous studies.[27–29]

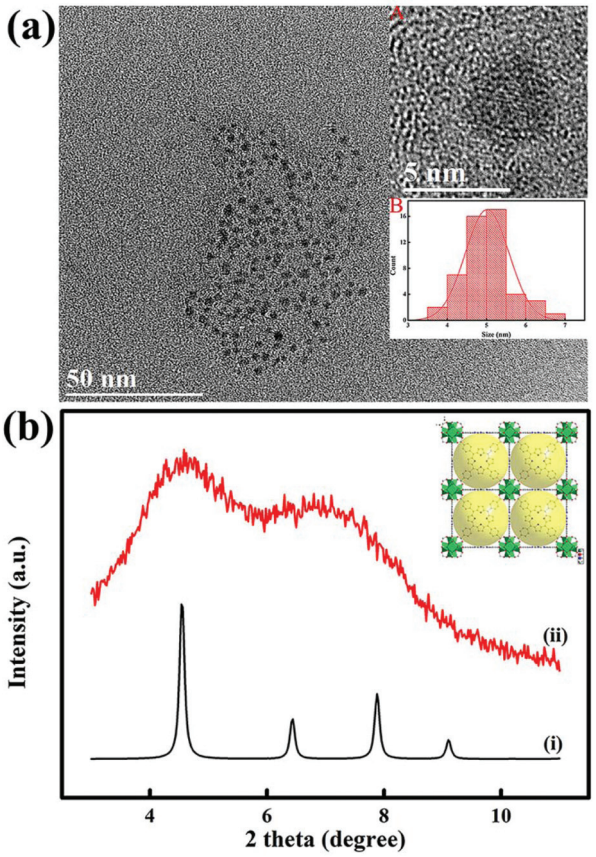


Fig. 2 (a) TEM image of the as-prepared MOF-525 NPs, insets: (A) single MOF-525 NP; (B) size distribution; (b) XRD patterns of (i) simulated MOF-525 and (ii) the as-prepared MOF-525 NPs, inset: the crystal structure of MOF-525.

Powder XRD measurement was then performed to identify the crystalline phase of the as-prepared sample. Fig. 2b shows the typical XRD pattern of the sample prepared in this work and the simulated XRD pattern of MOF-525.[25] The simulated XRD pattern of MOF-525 exhibited a prominent diffraction peak at 4.5° and other diffraction peaks at 6.4°, 7.8°, and 9.1° (Fig. 2b, pattern i). A distinct diffraction peak centered at 4.5° along with a shoulder peak covering the diffraction peaks at 6.4° and 7.8° could be observed for the as-prepared sample (Fig. 2b, pattern ii), which was consistent with the simulated XRD pattern of MOF-525. The diffraction peak centered at 9.1° was inconspicuous in the XRD pattern of the as-prepared sample, which might be attributed to the small size of the sample. The broad diffraction peaks were consistent with the small size characteristic as shown in Fig. 2a. Similar phenom-

ena have been reported in previous studies.[30,31] The aforementioned results demonstrated that ultrasmall MOF-525 NPs were successfully prepared *via* a hydrothermal approach by using water as the green solvent instead of dimethylformamide, which was widely employed in the previous work.[25]

The optical properties of MOF-525 NPs in the HEPES solution (20 mM, pH = 7.4) were investigated, as shown in Fig. 3a. The UV-Vis absorption spectrum of MOF-525 NPs exhibited a Soret band at 414 nm (curve a). It was observed that the fluorescence excitation spectrum of MOF-525 NPs was similar to the UV-Vis absorption spectrum (curve b). Under excitation at 414 nm, MOF-525 NPs would exhibit a strong emission peak at 646 nm and a shoulder peak centered at 704 nm, respectively (curve c). The inset of Fig. 3a shows the photographs of MOF-525 NPs dispersed in HEPES solution under (left) visible and (right) UV light. It could be clearly observed that MOF-525 NPs were dispersed well in the aqueous medium without apparent aggregation, which could be attributed to the ultrasmall size of MOF-525 NPs. In addition, the zeta potential of MOF-525 NPs was found to be *ca.* −30 mV, confirming again their good water dispersity (Fig. S1†). The characteristic red fluorescence of MOF-525 NPs was strong enough to be observed easily by the naked eye under UV light (inset of Fig. 3a). Inspired by the intense fluorescence and excellent water dispersity, it is anticipated that MOF-525 NPs would be potentially exploited as an efficient fluorescent probe in the sensing field. For this purpose, as one of the major concerns in fluorescent sensors, the fluorescence stability of MOF-525 NPs was investigated by monitoring the change in the fluorescence intensity at 646 nm. As shown in Fig. 3b, no obvious photobleaching behavior was observed and the fluorescence signal was quite stable with a relative standard deviation of 0.32%, which validated the feasibility of MOF-525 NPs as a fluorescent probe for sensor construction.

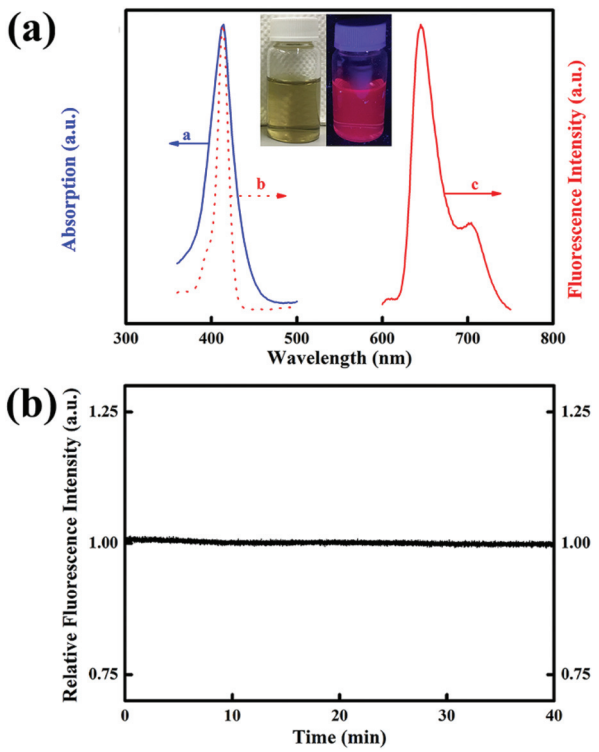


Fig. 3 (a) UV-Vis absorption, fluorescence excitation and emission spectra of MOF-525 NPs, inset: photographs of MOF-525 NPs under (left) visible and (right) UV light; (b) fluorescence stability testing of MOF-525 NPs.

### Fluorescence sensing of $Cu^{2+}$ in aqueous solution

Fig. S2† shows the time-dependent fluorescence response of MOF-525 NPs to $Cu^{2+}$. The fluorescence intensity of MOF-525 NPs decreased gradually with time upon the addition of 250 nM $Cu^{2+}$ and tended to reach a plateau in *ca.* 180 min, indicating the complete reaction between MOF-525 NPs and $Cu^{2+}$. As such, 180 min was chosen as the incubation time for MOF-525 NPs and $Cu^{2+}$ in the subsequent experiments. Fluorescence spectra of the MOF-525 NP dispersion in the presence of $Cu^{2+}$ with different concentrations were recorded. As shown in Fig. 4a, the fluorescence intensity decreased progressively with the increase of the $Cu^{2+}$ concentration in the range from 1.0 nM to 250 nM, while it decreased slightly upon further increas-

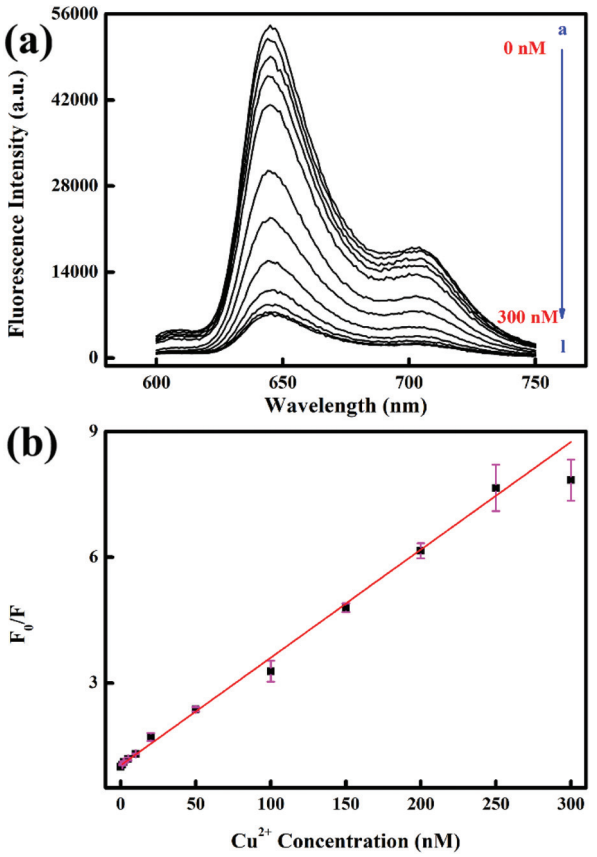


Fig. 4 (a) Fluorescence spectra of MOF-525 NPs (5 mg $L^{-1}$) in HEPES solution (20 mM, pH 7.4) under the excitation at 414 nm in the presence of $Cu^{2+}$ with different concentrations (a–l: 0–300 nM); (b) plot of $F_0/F$ against the concentration of $Cu^{2+}$, where $F_0$ and $F$ are the fluorescence intensities at 646 nm in the absence and presence of $Cu^{2+}$, respectively.

ing the $Cu^{2+}$ concentration. A similar trend was observed in the green fluorescent protein (GFP)-based fluorescent sensor for $Cu^{2+}$.[32] $F_0/F$ was used as an indicator to show the quenching effect of $Cu^{2+}$ on the fluorescence signal, where $F_0$ and $F$ are the fluorescence intensities at 646 nm in the absence and presence of $Cu^{2+}$, respectively. The correlation between $F_0/F$ and $Cu^{2+}$ concentration in aqueous solution is shown in Fig. 4b. A linear correlation between $F_0/F$ and $Cu^{2+}$ concentration from 1.0 nM to 250 nM was observed with a correlation coefficient of 0.9981. The detection limit was calculated to be as low as 220 pM. Furthermore, the Stern–Volmer equation was expressed as eqn (1):

$$F_0/F = K_{sv}[Q] + 1 \quad (1)$$

where $F_0$, $F$, $K_{sv}$ and [Q] represent the fluorescence intensity of the MOF-525 NP dispersion in the absence of $Cu^{2+}$, the fluorescence intensity of the MOF-525 NP dispersion in the presence of $Cu^{2+}$, the Stern–Volmer quenching constant and the molar concentration of $Cu^{2+}$, respectively. According to eqn (1), the Stern–Volmer quenching constant ($K_{sv}$) was estimated to be $2.56 \times 10^7$ $M^{-1}$, indicating the excellent quenching effect of $Cu^{2+}$ on the fluorescence of MOF-525 NPs. The aforementioned results demonstrated that the MOF-525 NP-based nanosensor for $Cu^{2+}$ detection had a high quenching constant and a low detection limit, which was somewhat better or comparable with other nanomaterial-based fluorescent sensors for $Cu^{2+}$ detection as shown in Table S1.† Herein, the potential applications of MOF NPs in the sensing field were expanded and an alternative sensing strategy towards $Cu^{2+}$ was proposed. More importantly, the MOF-525 NP-based fluorescent sensor for the detection of $Cu^{2+}$ could work in a totally aqueous medium, indicating its promising potential in the biological research field.

Not only sensitivity, but also selectivity was of great importance for the sensor. The possible interference of other common metal ions (*e.g.*, $Mg^{2+}$, $Zn^{2+}$, $Ca^{2+}$, $Cd^{2+}$, $Fe^{2+}$, $Fe^{3+}$, $Ni^{2+}$, $Ag^{+}$, $Al^{3+}$, $Hg^{2+}$, $Co^{2+}$, and $Pb^{2+}$) on the proposed fluorescent nanosensor was investigated. As shown in Fig. 5, a negligible quenching effect could be observed in the presence of $Mg^{2+}$, $Zn^{2+}$, $Ca^{2+}$, $Cd^{2+}$, $Fe^{2+}$, $Fe^{3+}$, $Ni^{2+}$, $Ag^{+}$, $Al^{3+}$, $Co^{2+}$ or $Pb^{2+}$, while $Hg^{2+}$ would quench the fluorescence intensity slightly. Similar phenomena were widely reported in the previous fluorescent sensors for $Cu^{2+}$.[13,15,32,33] However, the quenching effect of $Hg^{2+}$ was much weaker in comparison with that of $Cu^{2+}$. In addition, the quenching effect of $Cu^{2+}$ on the fluorescence intensity of MOF-525 NPs in the presence of these common metal ions was studied. It can be clearly observed that the quenching effect of $Cu^{2+}$ in the presence of $Mg^{2+}$, $Zn^{2+}$, $Ca^{2+}$, $Cd^{2+}$, $Fe^{2+}$, $Fe^{3+}$, $Ni^{2+}$, $Ag^{+}$, $Al^{3+}$, $Co^{2+}$ or $Pb^{2+}$ was similar to that of $Cu^{2+}$ alone, indicating that these metal ions exhibited negligible interference on the MOF-525 NP-based fluorescent nanosensor. Meanwhile, it is found that the quenching effect of $Cu^{2+}$ could be enhanced slightly in the presence of $Hg^{2+}$, implying the slight interference of $Hg^{2+}$ on the proposed fluorescent nanosensor. Similar phenomena were reported in the previous fluorescent sensors for $Cu^{2+}$.[20,34] However, as stated by the World Health Organization (WHO), the acceptable content of $Hg^{2+}$ (6 ppb, 30 nM) was much lower than that of $Cu^{2+}$ (2 ppm, 31 μM) in drinking water. Thus, in the practical water sample (*e.g.*, drinking water) analysis, the interference of $Hg^{2+}$ on the MOF-525 NP-based fluorescent nanosensor for $Cu^{2+}$ may be insignificant. The great selectivity of this fluorescent nanosensor could be attributed to the much stronger affinity of $Cu^{2+}$ to nitrogen atoms in the porphyrin ligand. Similar phenomena were reported in the previous fluorescent sensors for $Cu^{2+}$.[14,19,20]

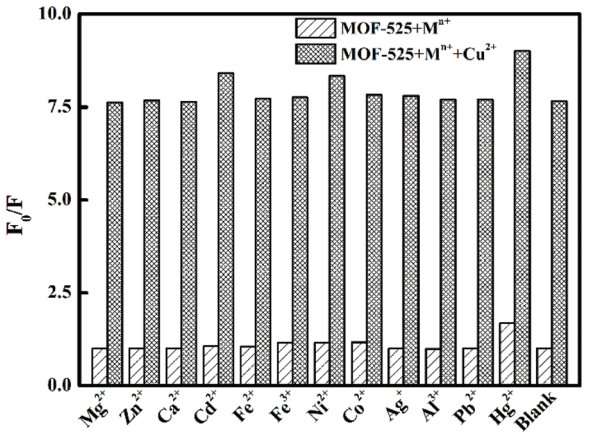


Fig. 5 The selectivity of an MOF-525 NP-based fluorescent nanosensor for $Cu^{2+}$ over other common metal ions. The concentration of each metal ion is 250 nM. $F_0$ and $F$ are the fluorescence intensities of MOF-525 NPs in the absence and presence of metal ions, respectively.

Furthermore, the potential of the MOF-525 NP-based sensitive and selective fluorescent nanosensor in practical applications was evaluated by the determination of $Cu^{2+}$ in drinking water. The water samples were spiked with known concentrations of $Cu^{2+}$ (0.00–150 nM) and analyzed by using the fluorescent nanosensor proposed in this work and by the inductively coupled plasma mass spectrometry (ICP-MS) method. As depicted in Table S2,† the proposed fluorescent nanosensor showed satisfactory recoveries in the range of 95.0% to 101.3%, and the $Cu^{2+}$ contents obtained from the proposed method were consistent with those obtained from the standard ICP-MS method, revealing great potential applications of the proposed fluorescent nanosensor with good reliability and accuracy in real sample analysis.

The possible response mechanism of the proposed fluorescent nanosensor for $Cu^{2+}$ was further explored. Generally, fluorescence quenching processes can be divided into two types: static quenching and dynamic quenching. Considering the large Stern–Volmer quenching constant ($2.56 \times 10^7$ $M^{-1}$), it was speculated that the fluorescence of MOF-525 NPs might be statically quenched by $Cu^{2+}$. According to the static quenching mechanism, the fluorescence lifetime of the fluorophore would not be affected by the quencher along with the formation of a nonfluorescent complex between the fluorophore and the quencher. Firstly, a time-resolved fluorescence lifetime

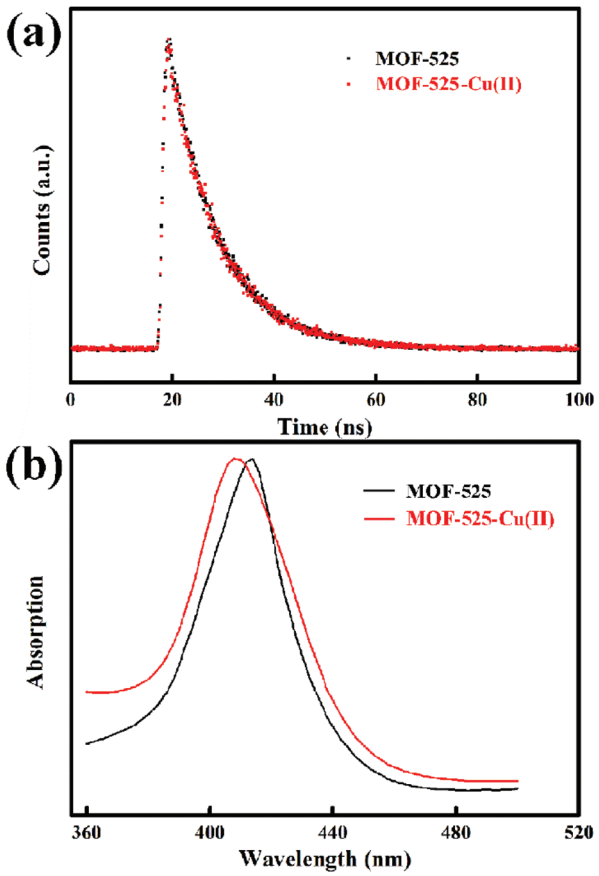


Fig. 6 (a) The time-resolved fluorescence decay curves and (b) the UV-Vis absorption spectra of the MOF-525 NP dispersion in the absence and presence of $Cu^{2+}$.

experiment was performed. The fluorescence decay curves of MOF-525 NPs in the absence and presence of $Cu^{2+}$ were obtained (Fig. 6a). The fluorescence lifetime values of MOF-525 NPs in the absence and presence of $Cu^{2+}$ were calculated to be 9.93 ns and 9.92 ns, respectively. Similar decay curves and fluorescence lifetime values revealed that the quenching process was predominantly static quenching. As shown in Fig. 1, the free-base porphyrin center in MOF-525 NPs would coordinate with $Cu^{2+}$ along with the formation of a nonfluorescent complex. Secondly, it was observed that the UV-Vis absorption spectrum of the MOF-525 NP dispersion would show a blue shift upon the addition of $Cu^{2+}$ (Fig. 6b). This blue shift of the UV-Vis absorption spectrum was due to the formation of the MOF-525-Cu(II) complex, which was also observed during the binding of $Cu^{2+}$ with other porphyrinic ligands.[35] As is well known, the fluorescence of MOF-525 NPs would originate from the porphyrin ligand (*i.e.*, TCPP). In addition, it is reported that the strong fluorescence signal of TCPP could be quenched in the presence of $Cu^{2+}$ due to the coordination between $Cu^{2+}$ and the nitrogen in TCPP.[14] Therefore, it is speculated that the free-base porphyrin centers in MOF-525 NPs would probably serve as the recognition sites for $Cu^{2+}$ due to the strong affinity of $Cu^{2+}$ to the nitrogen atom in the porphyrin center. In the presence of $Cu^{2+}$, the porphyrin center in fluorescent MOF-525 NPs would react with $Cu^{2+}$, followed by the formation of a nonfluorescent complex, MOF-525-Cu(II), resulting in the fluorescence "Signal-Off" response of the proposed nanosensor to $Cu^{2+}$. A similar result was reported in the previous work.[20]

### Intracellular imaging of $Cu^{2+}$ in living cells

Owing to the unique properties of MOF-525 NPs including ultrasmall size, good water dispersity, good photostability and intense fluorescence, it was anticipated that the MOF-525 NP-based fluorescent nanosensor could be an excellent candidate for the intracellular imaging of $Cu^{2+}$. In order to confirm this possibility, the cytotoxicity of MOF-525 NPs was firstly investigated by MTT assays (Fig. S2†). No obvious cytotoxicity against HeLa cells was observed (viability over 80%) when the concentration of MOF-525 NPs was below 30 mg $L^{-1}$, demonstrating the acceptable biocompatibility, low cytotoxicity and great potential in cell imaging. Then, the potential application of MOF-525 NPs for intracellular imaging of $Cu^{2+}$ was studied in living HeLa cells. As shown in Fig. 7a, HeLa cells before incubation with MOF-525 NPs did not show an obvious fluorescence signal. Significant red fluorescence could be observed

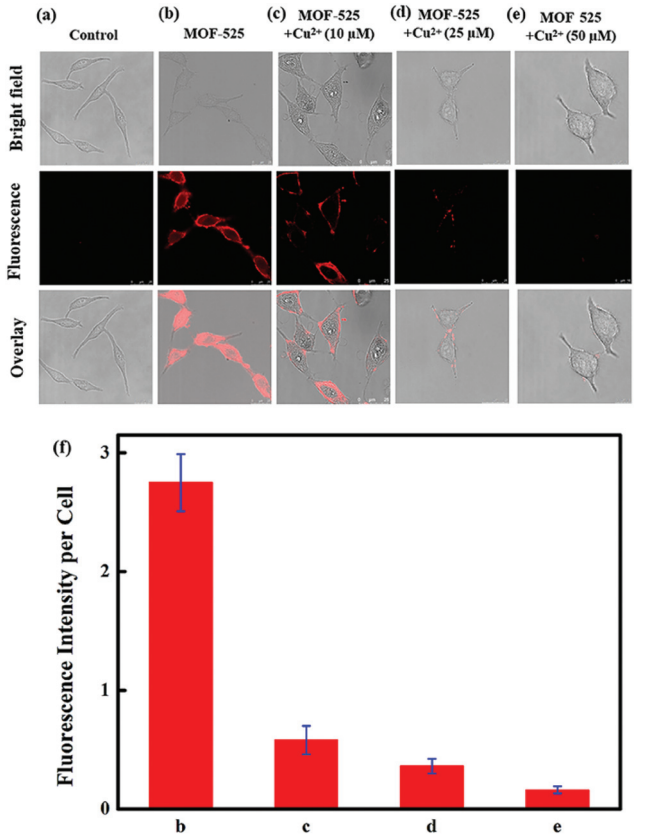


Fig. 7 Confocal fluorescence images of HeLa cells with (a) no treatment and in the presence of (b) MOF-525 NPs (30 mg $L^{-1}$); (c) MOF-525 NPs and 10 μM $Cu^{2+}$; (d) MOF-525 NPs and 25 μM $Cu^{2+}$; and (e) MOF-525 NPs and 50 μM $Cu^{2+}$. (f) The corresponding fluorescence intensity per cell in confocal fluorescence images b, c, d, and e.

in HeLa cells after incubation with MOF-525 NPs at a concentration of 30 mg $L^{-1}$ (Fig. 7b and f). These results confirmed the penetration of MOF-525 NPs into living cells. MOF-525 labelled HeLa cells were then incubated with exogenous $Cu^{2+}$ at different concentrations (*i.e.*, 10 μM, 25 μM and 50 μM) for 30 min. The quantified mean fluorescence intensity per cell for various $Cu^{2+}$ concentrations was analyzed using ImageJ software. Fluorescence image signals of HeLa cells gradually became weaker in a $Cu^{2+}$ concentration-dependent manner until complete quenching (Fig. 7c–f). These results demonstrated the capability of the fluorescent nanosensor in $Cu^{2+}$ imaging in living cells.

## Conclusions

In the present work, a porphyrinic MOF nanoparticle (MOF-525 NP)-based fluorescent nanosensor was successfully proposed for $Cu^{2+}$ sensing in aqueous solution with a wide linear range (1.0–250 nM), a low detection limit (220 pM) and a high quenching constant ($2.56 \times 10^7$ $M^{-1}$). Furthermore, this MOF-525 NP based fluorescent sensor has been successfully used for $Cu^{2+}$ monitoring in water samples and living HeLa cells. The present research would offer an alternative fluorescence sensing and intracellular imaging strategy for $Cu^{2+}$, and expand the potential applications of MOFs in the fields of sensing and bioimaging.

## Conflicts of interest

There are no conflicts to declare.

## Acknowledgements

This work was supported by the National Natural Science Foundation of China (NSFC) (No. 21976166, 31771077, and 21405144), the Science Challenge Project (TZ2016004), the General Research fund (GRF) of Research Grant Council of Hong Kong (15210818), and The Hong Kong Polytechnic University Internal Fund (1-ZVJ7 and 1-YW1L). This work was also supported by the University Research Facility in Life Sciences of The Hong Kong Polytechnic University.

## References

1 O. Bandmann, K. H. Weiss and S. G. Kaler, *Lancet Neurol.*, 2015, **14**, 103–113.
2 H. Si, R. Sheng, Q. Li, J. Feng, L. Li and B. Tang, *Anal. Chem.*, 2018, **90**, 8785–8792.
3 M. Zhan, H. Jia, J. Fan, H. Yu, E. Amador and W. Chen, *Anal. Chem.*, 2019, **91**, 6103–6110.
4 S. Takano, M. Tanimizu, T. Hirata and Y. Sohrin, *Anal. Chim. Acta*, 2013, **784**, 33–41.
5 S. V. Smirnova, T. O. Samarina, D. V. Ilin and I. V. Pletnev, *Anal. Chem.*, 2018, **90**, 6323–6331.
6 C. Cheng, Y. Huang, X. Tian, B. Zheng, Y. Li, H. Yuan, D. Xiao, S. Xie and M. M. F. Choi, *Anal. Chem.*, 2012, **84**, 4754–4759.
7 J. Zhang, C. Cheng, Y. Huang, L. Qian, B. Zheng, H. Yuan, Y. Guo and D. Xiao, *Analyst*, 2013, **138**, 2073–2079.
8 K. P. Carter, A. M. Young and A. E. Palmer, *Chem. Rev.*, 2014, **114**, 4564–4601.
9 S. Wang, C. Liu, G. Li, Y. Sheng, Y. Sun, H. Rui, J. Zhang, J. Xu and D. Jiang, *ACS Sens.*, 2017, **2**, 364–370.
10 Y. Jia, T. Sun, Y. Jiang, W. Sun, Y. Zhao, J. Xin, Y. Hou and W. Yang, *Analyst*, 2018, **143**, 5145–5150.
11 P. Jiang, S. Li, M. Han, Y. Liu and Z. Chen, *Analyst*, 2019, **144**, 2604–2610.
12 N. Y. Cheng, P. Jiang, Q. Liu, J. Q. Tian, A. M. Asiri and X. P. Sun, *Analyst*, 2014, **139**, 5065–5068.
13 Y. Song, D. Hu, F. Liu, S. Chen and L. Wang, *Analyst*, 2015, **140**, 623–629.
14 L. Lu, C. Feng, J. Xu, F. Wang, H. Yu, Z. Xu and W. Zhang, *Biosens. Bioelectron.*, 2017, **92**, 101–108.
15 C. Zou, M. F. Foda, X. Tan, K. Shao, L. Wu, Z. Lu, H. S. Bahlol and H. Han, *Anal. Chem.*, 2016, **88**, 7395–7403.
16 P. Kumar, A. Deep and K.-H. Kim, *TrAC, Trends Anal. Chem.*, 2015, **73**, 39–53.
17 K. Lu, T. Aung, N. Guo, R. Weichselbaum and W. Lin, *Adv. Mater.*, 2018, **30**, 1707634.
18 W. Cho, H. J. Lee, G. Choi, S. Choi and M. Oh, *J. Am. Chem. Soc.*, 2014, **136**, 12201–12204.
19 L. Li, S. Shen, R. Lin, Y. Bai and H. Liu, *Chem. Commun.*, 2017, **53**, 9986–9989.
20 J. Chen, H. Chen, T. Wang, J. Li, J. Wang and X. Lu, *Anal. Chem.*, 2019, **91**, 4331–4336.
21 Z. Lu, H. G. W. Godfrey, I. da Silva, Y. Cheng, M. Savage, F. Tuna, E. J. L. McInnes, S. J. Teat, K. J. Gagnon, M. D. Frogley, P. Manuel, S. Rudić, A. J. Ramirez-Cuesta, T. L. Easun, S. Yang and M. Schröder, *Nat. Commun.*, 2017, **8**, 14212.
22 X. Fang, Q. Shang, Y. Wang, L. Jiao, T. Yao, Y. Li, Q. Zhang, Y. Luo and H.-L. Jiang, *Adv. Mater.*, 2018, **30**, 1705112.
23 K. Li, S. Lin, Y. Li, Q. Zhuang and J. Gu, *Angew. Chem., Int. Ed.*, 2018, **57**, 3439–3443.
24 R. Röder, T. Preiß, P. Hirschle, B. Steinborn, A. Zimpel, M. Höhn, J. O. Rädler, T. Bein, E. Wagner, S. Wuttke and U. Lächelt, *J. Am. Chem. Soc.*, 2017, **139**, 2359–2368.
25 W. Morris, B. Volosskiy, S. Demir, F. Gándara, P. L. McGrier, H. Furukawa, D. Cascio, J. F. Stoddart and O. M. Yaghi, *Inorg. Chem.*, 2012, **51**, 6443–6445.
26 A. Zhu, Q. Qu, X. Shao, B. Kong and Y. Tian, *Angew. Chem., Int. Ed.*, 2012, **51**, 7185–7189.
27 J. Wang, Y. Fan, H. Lee, C. Yi, C. Cheng, X. Zhao and M. Yang, *ACS Appl. Nano Mater.*, 2018, **1**, 3747–3753.
28 J. Park, Q. Jiang, D. Feng, L. Mao and H. Zhou, *J. Am. Chem. Soc.*, 2016, **138**, 3518–3525.
29 J. Zhuang, C. H. Kuo, L. Y. Chou, D. Y. Liu, E. Weerapana and C. K. Tsung, *ACS Nano*, 2014, **8**, 2812–2819.

30 W. Liu, Y. Wang, Y. Li, S. Cai, X. Yin, X. He and Y. Zhang, *Small*, 2017, **13**, 1603459.
31 U. Ryu, S. Jee, J.-S. Park, I. K. Han, J. H. Lee, M. Park and K. M. Choi, *ACS Nano*, 2018, **12**, 4968–4975.
32 C. Lei, Z. Wang, Z. Nie, H. Deng, H. Hu, Y. Huang and S. Yao, *Anal. Chem.*, 2015, **87**, 1974–1980.
33 Y. Q. Dong, R. X. Wang, G. Li, C. Q. Chen, Y. W. Chi and G. N. Chen, *Anal. Chem.*, 2012, **84**, 6220–6224.
34 X. M. Lin, G. M. Gao, L. Y. Zheng, Y. W. Chi and G. N. Chen, *Anal. Chem.*, 2014, **86**, 1223–1228.
35 A. Hopt, S. Korte, H. Fink, U. Panne, R. Niessner, R. Jahn, H. Kretzschmar and J. Herms, *J. Neurosci. Methods*, 2003, **128**, 159–172.